Science Advances
AAAS

Supplementary Materials for

Structure of S1PR2–heterotrimeric G_{13} signaling complex

Hongwen Chen, Kevin Chen, Weijiao Huang, Louis M. Staudt, Jason G. Cyster*, Xiaochun Li*

*Corresponding author. Email: jason.cyster@ucsf.edu (J.G.C.); xiaochun.li@utsouthwestern.edu (X.L.)

Published 30 March 2022, *Sci. Adv.* **8**, eabn0067 (2022)
DOI: 10.1126/sciadv.abn0067

This PDF file includes:

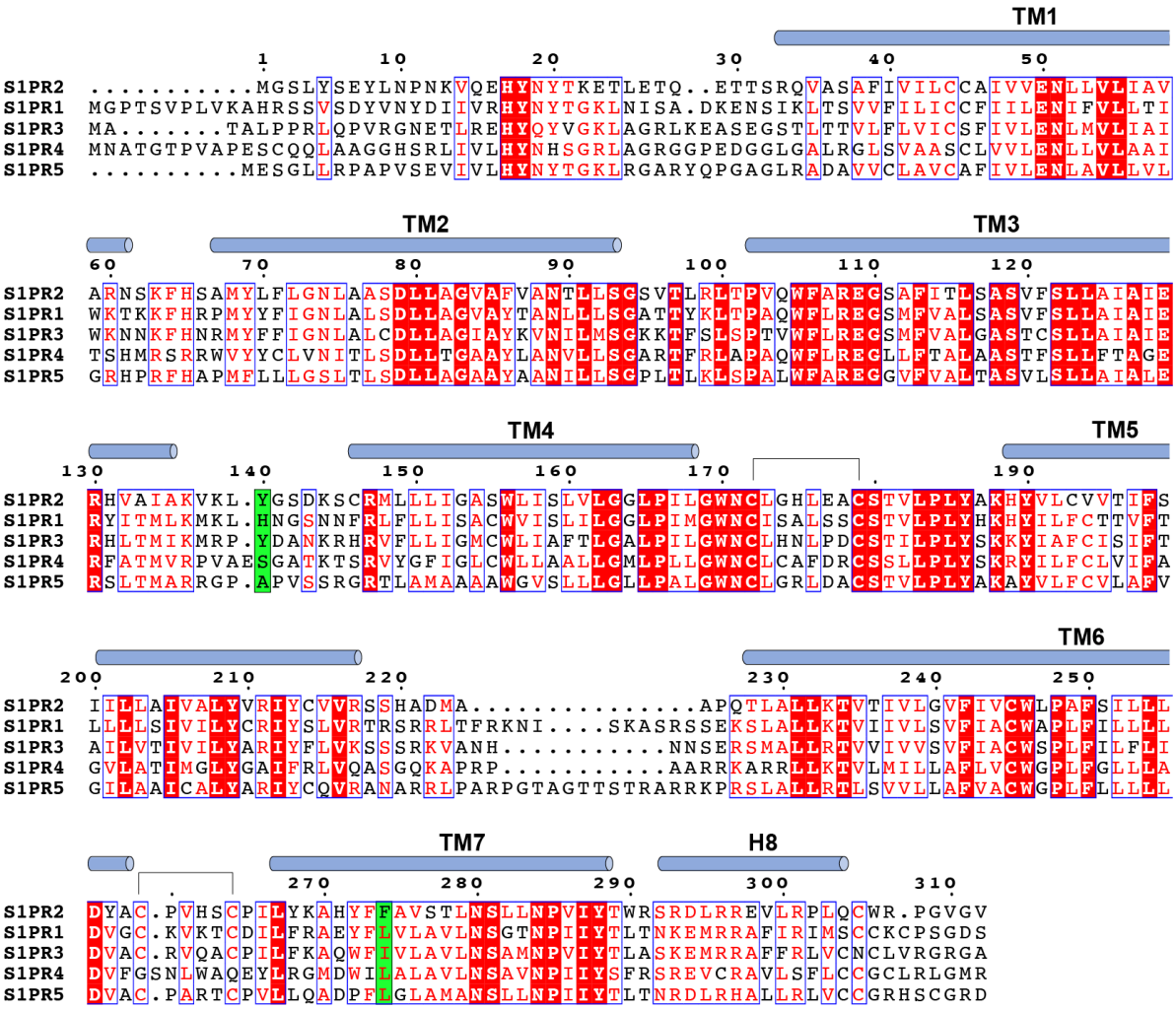

Fig. S1 Sequence alignment of human S1PR1, S1PR2, S1PR3, S1PR4 and S1PR5. The transmembrane helices and the residue numbers of human S1PR2 are indicated above the protein sequences. The conserved residues are highlighted in red and the unique residues of S1PR2 are highlighted in green.

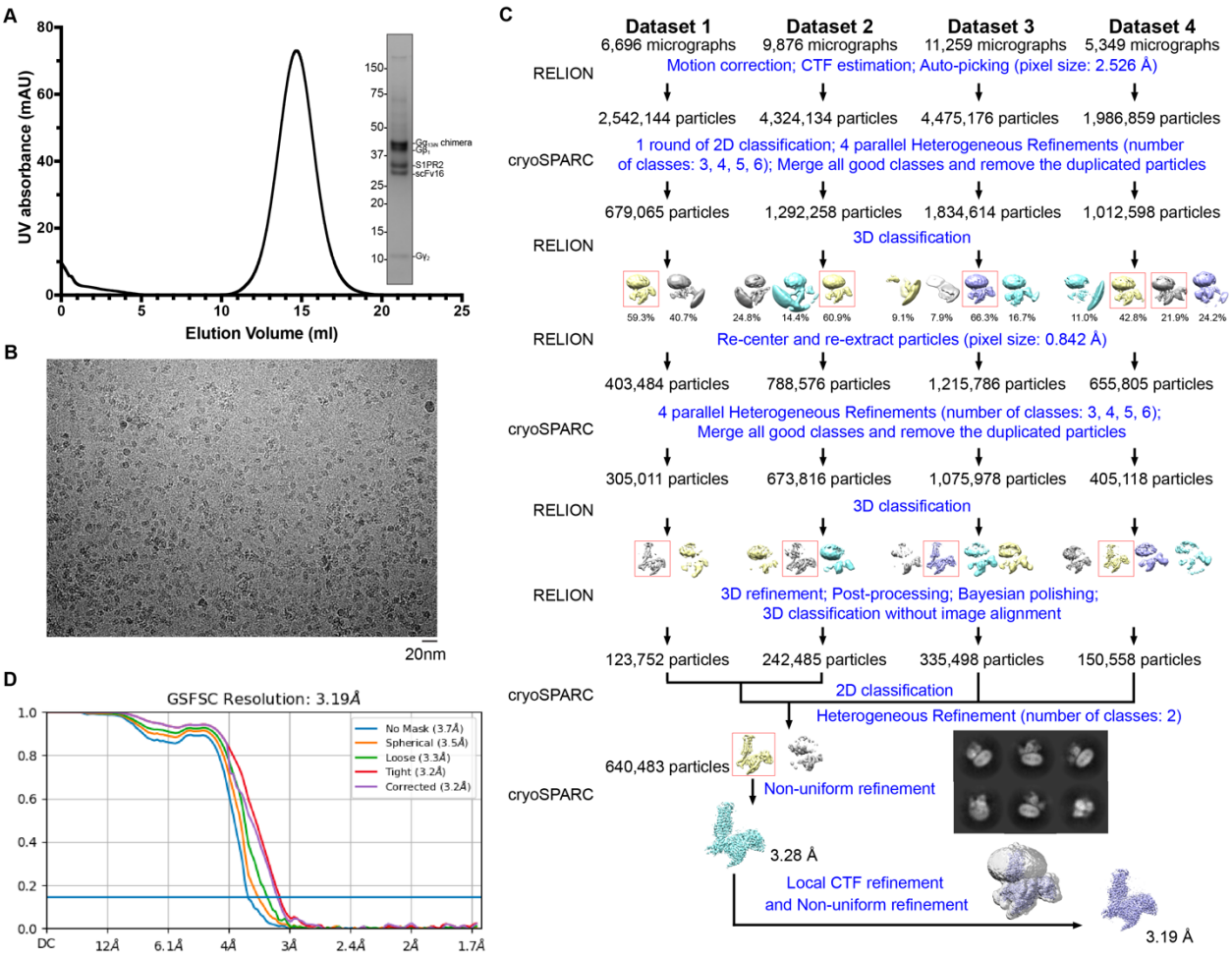

Fig. S2 Data processing for data acquired.

(A) Representative Superose 6 increase 10/30 gel-filtration chromatogram of S1PR2-G_{13}-scFv16 complex. The peak fraction is shown on SDS-PAGE with molecular markers. **(B)** A representative electron micrograph at a defocus of −2.0 μm. **(C)** The data processing workflow. The cryo-EM 3D classes and refinement results are shown. 2D classification from cryoSPARC is shown. **(D)** Fourier shell correlation (FSC) curve as a function of resolution using cryoSPARC output.

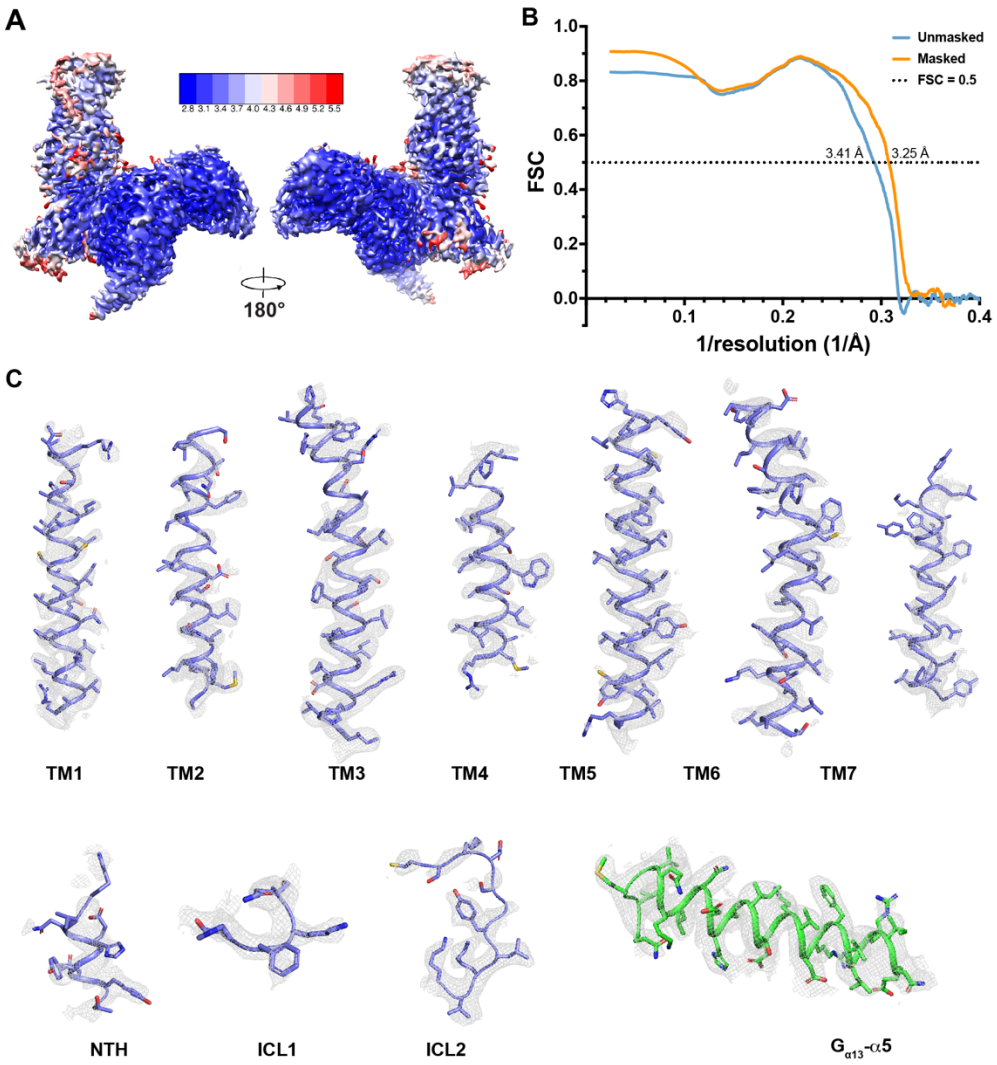

Fig. S3 cryo-EM map of structural elements.

(A) Density maps of structure colored by local resolution estimation using cryoSPARC. **(B)** The FSC curves calculated between the refined structure model and the half map used for refinement. **(C)** The major structural elements of S1PR2-G_{13}-scFv16 complex. EM density map and model of the complex are shown in mesh and cartoon.

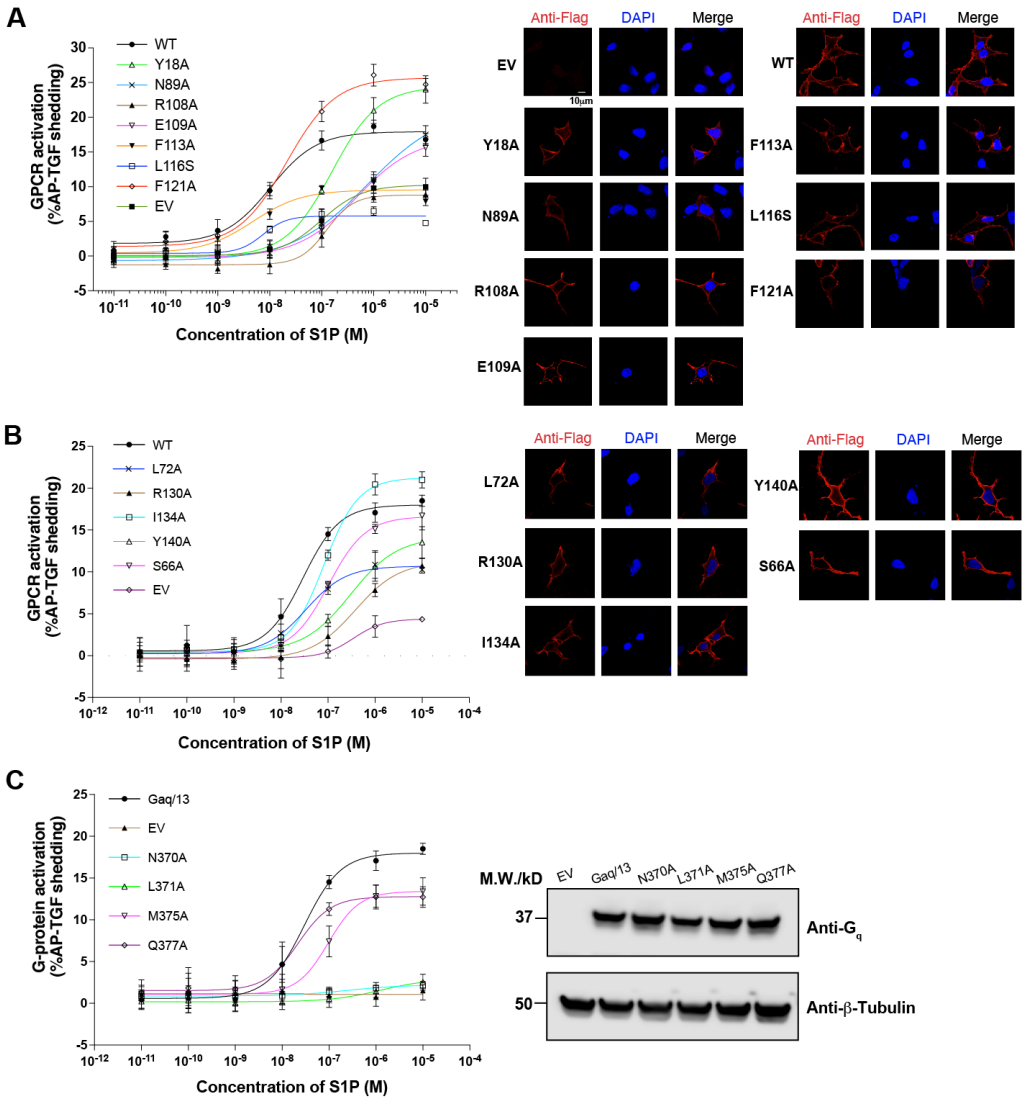

Fig. S4 Surface Expression of S1PR2 and expression levels of $G_{\alpha q/13}$ variants in this study. **(A)** Mutagenesis analysis of residues for engaging d18:1 S1P. Wild-type (WT) S1PR2, empty vector (EV) and mutants were examined for d18:1 S1P-induced AP-TGFα shedding responses in the HEK293Δ$G_{q/11/12/13}$ cell line reflecting G_{13} signaling. The representative dose-response curves from same-day experiment are shown. Data are mean ± s.d. (n=3). **(B)** Mutagenesis analysis of S1PR2 residues for engaging $G_{\alpha 13}$-α5. The representative dose-response curves from same-day experiment are shown. Data are mean ± s.d. (n=3). The surface expressed S1PR2 proteins were detected by immunofluorescence staining. **(C)** Mutagenesis analysis of $G_{\alpha 13}$ residues for engaging S1PR2. The representative dose-response curves from same-day experiment are shown. Data are mean ± s.d. (n=3). β-tubulin served as an internal control and was detected via anti-β- tubulin antibody.

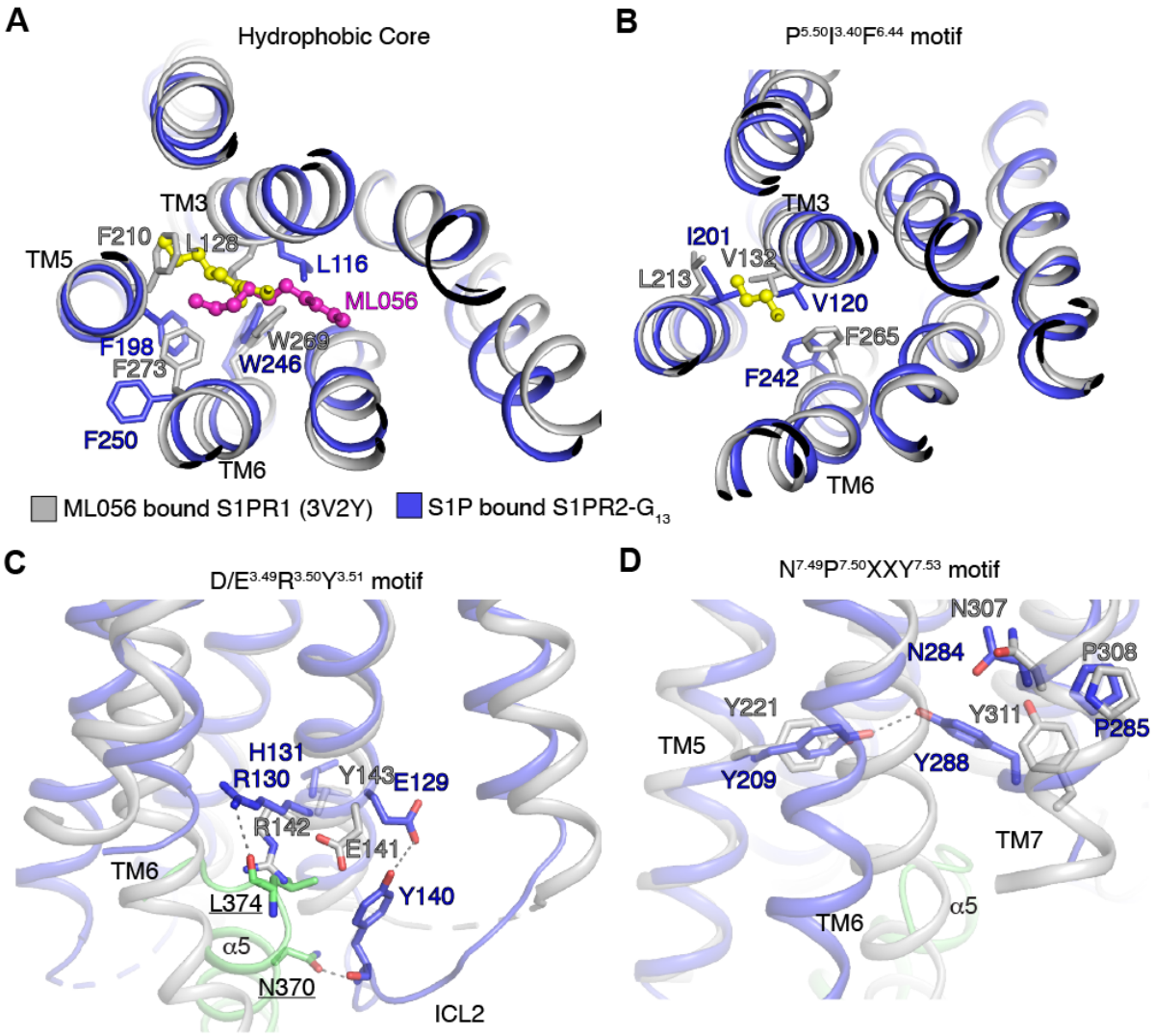

Fig. S5 Structural Comparisons of S1PR2 (blue) and inactive S1PR1 (gray).

(A) Comparison of the ligand binding pockets. The S1P in the S1PR2 structure is shown in yellow sticks and the S1PR1 antagonist ML056 is shown in magenta sticks. **(B)** Comparison of the PIF motif of both structures. **(C)** Comparison of the DRY motif of both structures. **(D)** Comparison of the NPXXY motif of both structures. The hydrophilic interactions are indicated by dashed lines. The crucial residues are labeled and shown as sticks. The residues of $G_{\alpha 13}$-α5 are underlined.

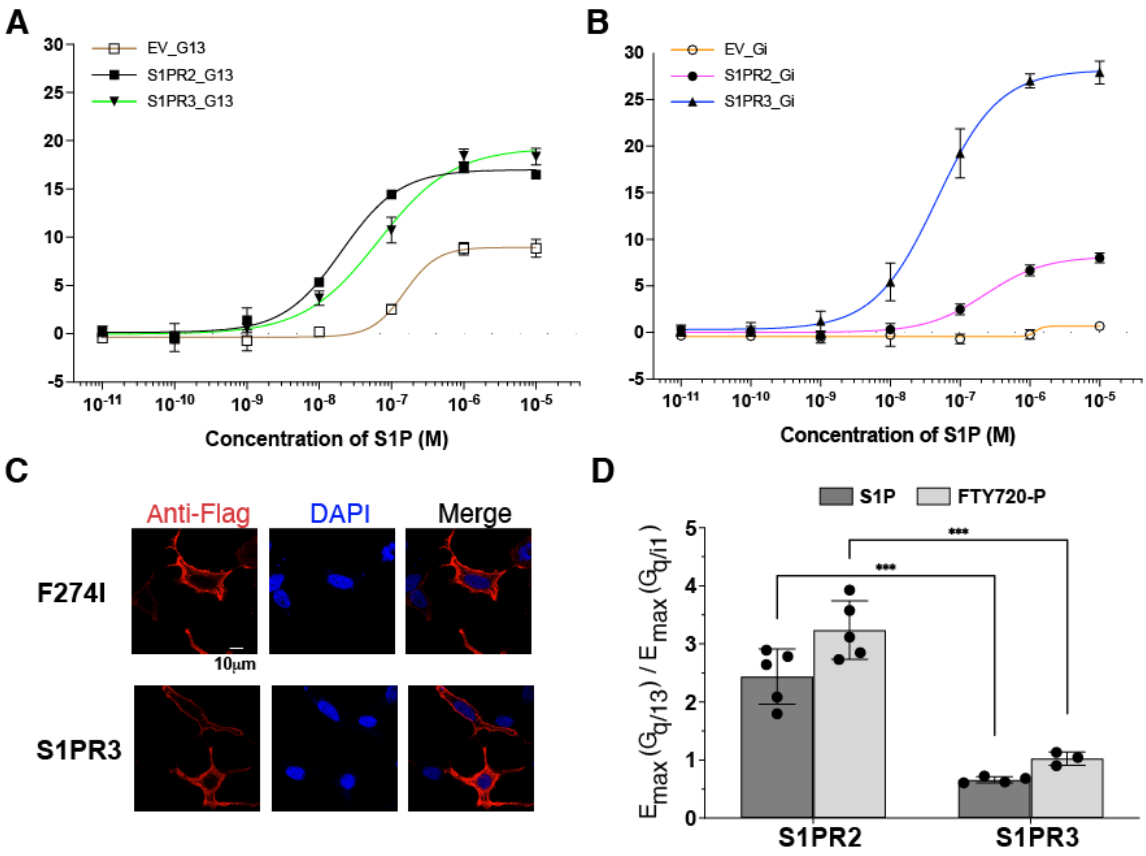

Fig. S6 S1P triggers the activation of G_i and G_{13} via S1PR2 and S1PR3.

(A-B) Wild-type (WT) S1PR2, S1PR3 and empty vector (EV) were examined for d18:1 S1P-induced AP-TGFα shedding responses in the HEK293Δ$G_{q/11/12/13}$ cell line reflecting G_{13} **(A)** or G_{i1} **(B)** signaling. The representative dose-response curves from same-day experiment are shown. Data are mean ± s.d. (n=3). **(C)** The surface expression of $S1PR2^{F274I}$ and S1PR3. The surface expressed S1PRs were detected by immunofluorescence staining. **(D)** The ratio of maximal $G_{q/13}$-dependent % AP-TGFα shedding versus maximal $G_{q/i1}$-dependent % AP-TGFα shedding. S1PR2 shows $G_{q/13}$-biased activity compared with wild-type S1PR3. Data are mean ± s.d. (n=3-5 independent experiments) and analyzed using unpaired Students' t-test (***P<0.001).

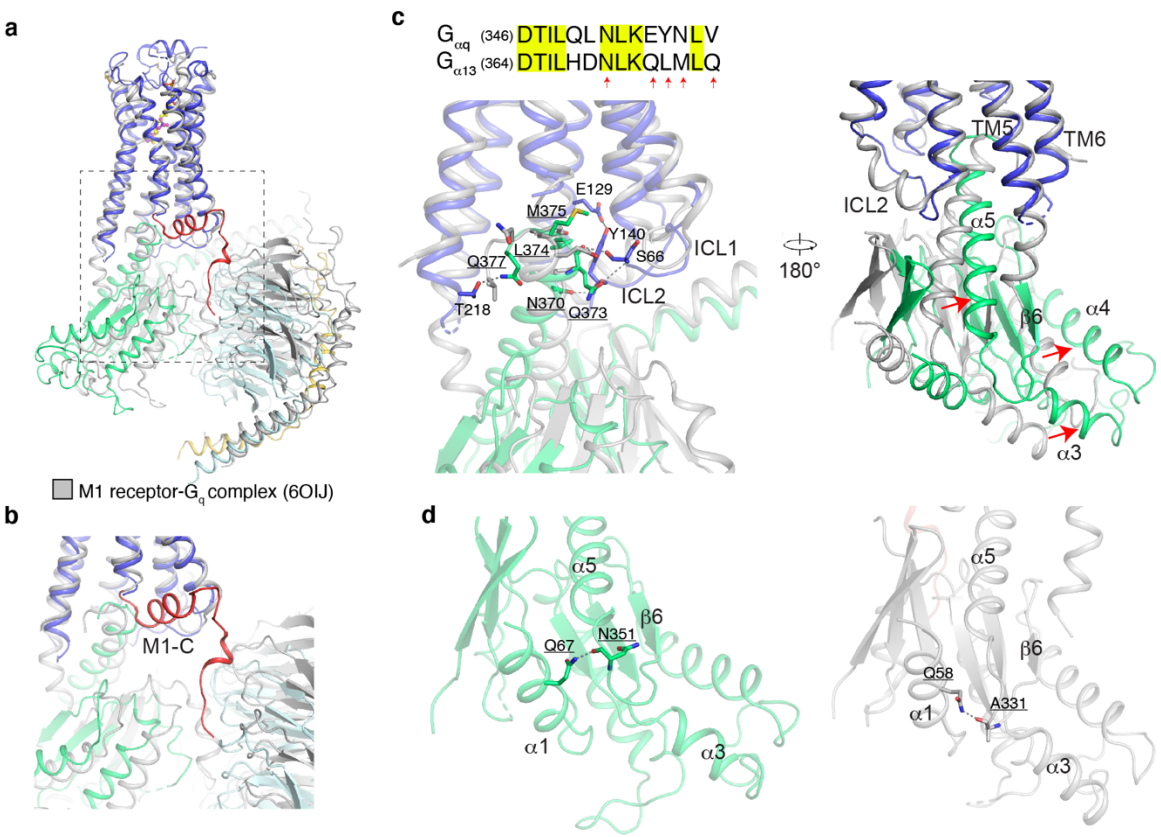

Fig. S7 Structural Comparison of S1PR2-G_{13} complex and M1 receptor-G_q complex.

(A) Comparison of the overall structures. **(B)** Comparison of C-terminus of M1 (red) with that of S1PR2. **(C)** Comparison of the receptor-G protein interface of both structures. The sequence alignment of α5 is shown. The structural difference between $G_{\alpha q}$ and $G_{\alpha 13}$ is indicated by arrows. The hydrophilic interactions are indicated by dashed lines. The crucial residues are labeled and shown as sticks. The residues of $G_{\alpha 13}$-α5 are underlined. **(D)** Comparison of the interactions between residue Gln in α1 and the β6-α5 loop.

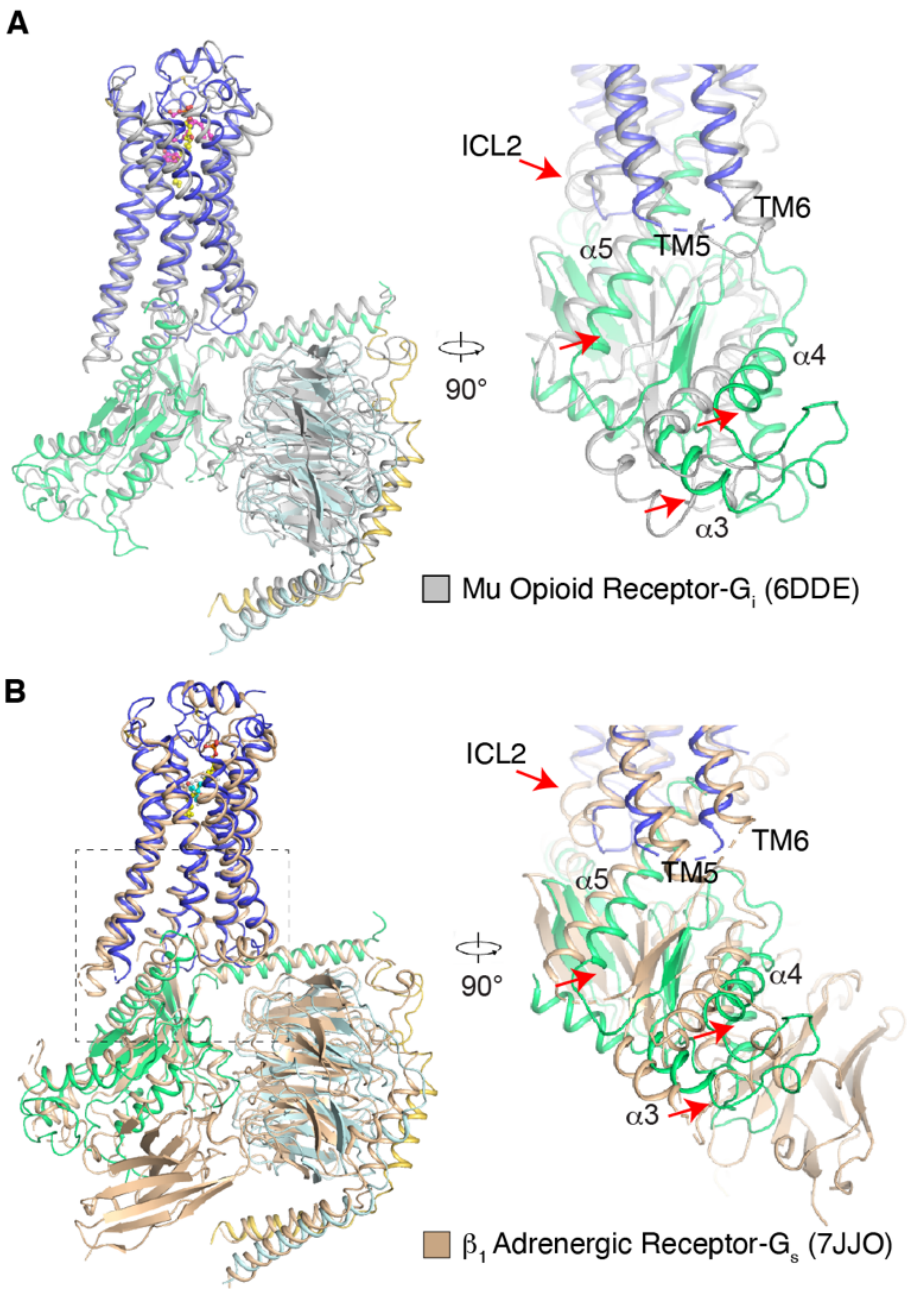

Fig. S8 Structural Comparisons of S1PR2-G_{13} complex with μ receptor-G_i complex and β1-G_s complex.

(A) Comparison of the S1PR2-G_{13} complex with μ receptor-G_i complex. **(B)** Comparison of S1PR2-G13 complex and β1-G_s complex.

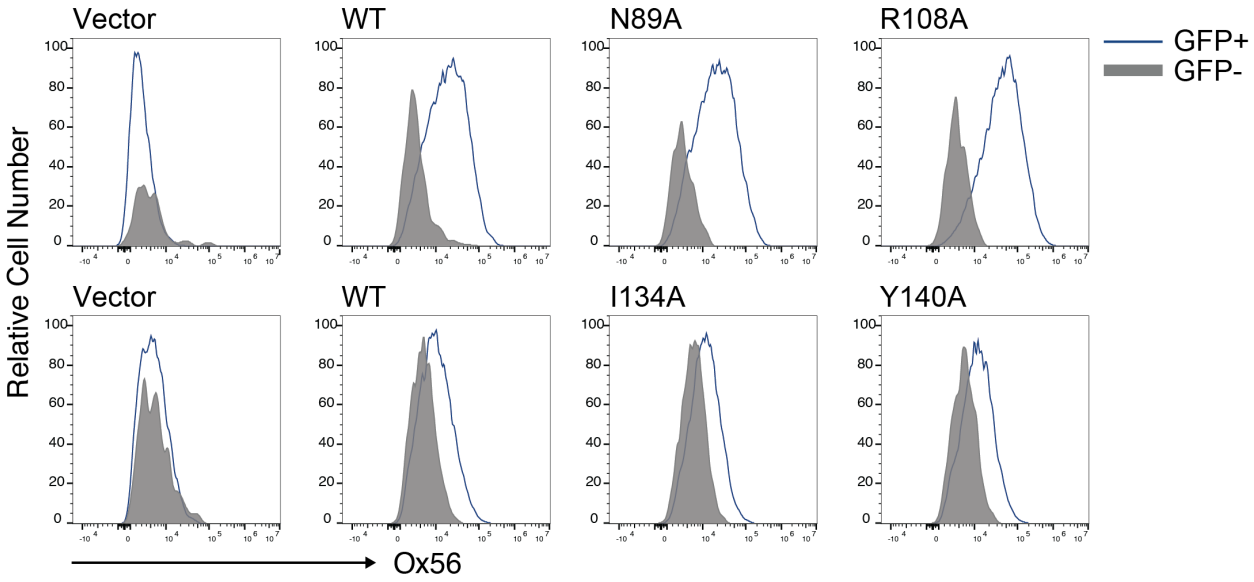

Fig. S9 Representative FACS plots of S1PR2 transduced WEHI231 B lymphoma cells.

S1PR2 wild-type, S1PR2 variant or control (Vector) expressing WEHI-231 cells were stained with Ox56 antibody to detect surface levels of the receptor. GFP was used to identify transduced cells. Ox56 staining of untransduced GFP- cells provides a staining control. Analyses in upper and lower row were done on different days, accounting for the different staining intensities.

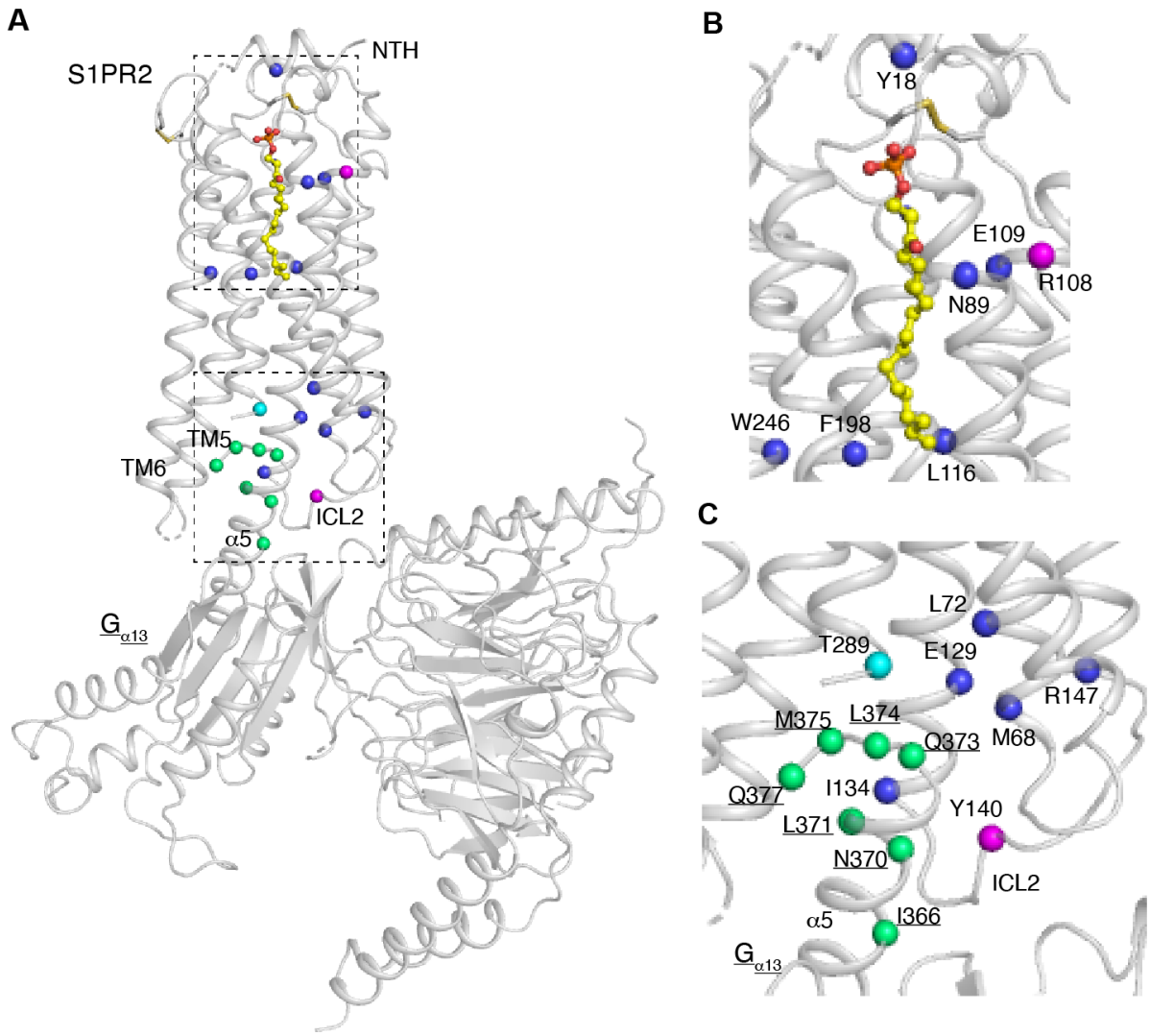

Fig. S10 Distribution of disease-causing mutations in the S1PR2-G_{13} complex.

(A) Distribution of disease-causing mutations in the overall complex structure. Mutations in S1PR2 are highlighted in blue (GCB-DLBCL only), cyan (hearing loss only) and magenta (GCB-DLBCL and hearing loss); mutations in $G_{\alpha 13}$ are highlighted in green (GCB-DLBCL only). **(B)** Distribution of disease-causing mutations in the S1P binding site. **(C)** Distribution of disease-causing mutations in the receptor and $G_{\alpha 13}$ interface. The S1P is shown as yellow sticks. The residues are shown in spheres and the residues of $G_{\alpha 13}$ are underlined.

Table S1 Cryo-EM data collection, refinement and validation statistics

	S1PR2-G_{13} complex (EMDB-25712) (PDB-7T6B)
Data collection and processing	
Magnification	60024
Voltage (kV)	300
Electron exposure (e–/Å^2)	60
Defocus range (μm)	-1.0 to -2.0
Pixel size (Å)	0.842
Symmetry imposed	C1
Initial particle images (no.)	13,328,313
Final particle images (no.)	640,483
Map resolution (Å)	3.2
FSC threshold	0.143
Refinement	
Model resolution (Å)	3.3
FSC threshold	0.5
Map sharpening *B* factor (Å^2)	-152
Model composition	
Non-hydrogen atoms	8755
Protein residues	1119
Ligands	1
B factors (Å^2)	
Protein	69.78
Ligand	110.83
R.m.s. deviations	
Bond lengths (Å)	0.004
Bond angles (°)	0.746
Validation	
MolProbity score	1.62
Clashscore	6.29
Poor rotamers (%)	0.21
Ramachandran plot	
Favored (%)	96.00
Allowed (%)	4.00
Disallowed (%)	0